Incoherent dynamics in the toric code subject to disorder

Beat Röthlisberger,[1] James R. Wootton,[1,2] Robert M. Heath,[2] Jiannis K. Pachos,[2] and Daniel Loss[1]
[1]*Department of Physics, University of Basel, Klingelbergstrasse 82, CH-4056 Basel, Switzerland*
[2]*School of Physics and Astronomy, University of Leeds, Leeds LS2 9JT, United Kingdom*
(Received 18 January 2012; published 13 February 2012)

We numerically study the effects of two forms of quenched disorder on the anyons of the toric code. First, a class of codes based on random lattices of stabilizer operators is presented and shown to be superior to the standard square-lattice toric code for certain forms of biased noise. It is further argued that these codes are close to optimal, in that they tightly reach the upper bound of error thresholds beyond which no correctable Calderbank-Shore-Steane codes can exist. Additionally, we study the classical motion of anyons in toric codes with randomly distributed on-site potentials. In the presence of repulsive long-range interaction between the anyons, a surprising increase in the lifetime of encoded states with disorder strength is reported and explained by an entirely incoherent mechanism. Finally, the coherent transport of the anyons in the presence of both forms of disorder is investigated and a significant suppression of the anyon motion is found.

DOI: 10.1103/PhysRevA.85.022313 PACS number(s): 03.67.Pp, 03.67.Lx, 05.50.+q, 72.15.Rn

I. INTRODUCTION

A working quantum computer performing meaningful calculations unarguably requires information processing to be carried out in a fault-tolerant manner [1,2]. This means not only protecting the information from the action of imperfect gates, but also storing it in a reliable way during the course of computation. In the theory of quantum error correction, the state of a logical qubit can be encoded in the code space of a number of physical qubits [3]. The resulting redundancy allows one to implement fault-tolerant quantum gates and to periodically check for the occurrence of single-qubit errors using syndrome measurements. However, this kind of active error monitoring imposes an additional overhead on an already deeply involved vision. Therefore, the idea of manipulating and storing quantum states in systems that already provide "built-in" protection from errors has gained a lot of attention recently [4–7]. A promising approach in this direction is to encode information in the degenerate topologically ordered ground state of a suitable many-body Hamiltonian. Information is encoded in an entangled state distributed across a large number of qubits and can be distinguished and modified only in a nonlocal manner. In this context, Kitaev's toric code [4] is arguably the best-studied model to date. It is robust against local perturbation at zero temperature, as well as against thermal errors if long-range interaction between its fundamental excitations is present [8–10].

Recent studies have focused on coherent phenomena in the toric code that arise due to the additional presence of various forms of quenched disorder [11–14]. Conversely, this work is primarily concerned with a numerical study of incoherent (classical) effects caused by two particular forms of randomness. First, we consider a class of models similar to the toric code, but differing from the latter in that the syndrome check operators are chosen randomly from a set of three-body and six-body operators. These correspond to a generalization of the (square-lattice) toric code to randomized lattices. We find that these models have an advantage over the toric code for biased noise, where bit-flip and phase-flip errors occur with different probabilities. We also present strong evidence that these codes are almost optimal, in the sense that they reach error thresholds close to the overall upper bound valid for any Calderbank-Shore-Steane (CSS) code [15,16]. Second, we investigate the effect of random on-site potentials on the lifetime of states encoded in the regular toric code coupled to a thermal bath. We identify and describe an interesting regime, where, in the presence of long-range interactions, the lifetime of this quantum memory is enhanced for increasing disorder strength. Finally, the effects of the random lattices on coherent anyon transport are investigated, both with and without additional randomness in the on-site potentials. The resultant slowdown of the anyonic motion is determined and its effect on the stability of the quantum memory is discussed.

The paper is organized as follows: Section II reviews the toric code, which is the basis of all further studies in this work. We then show in Sec. III how to simulate the classical dynamics of excitations in the systems considered subsequently and also give some details of the numerics. Our main results are presented in Secs. IV, V, and VI, followed by a conclusion in Sec. VII.

II. REVIEW OF THE TWO-DIMENSIONAL TORIC CODE

The starting point of our investigation is Kitaev's two-dimensional (2D) toric code [4] which will be modified in the following sections to incorporate randomness. We provide here a brief outline of the original model for the sake of completeness. The 2D toric code consists of $2L^2$ spins $\frac{1}{2}$ with each spin placed on an edge of an underlying $L \times L$ square lattice with periodic boundary conditions. One then defines two sets of mutually commuting four-body operators, called plaquettes and stars, respectively, in the following way [see Fig. 1(a)]. A plaquette is the product of the Pauli σ_z operators associated with the four spins belonging to a single face of the square lattice, whereas a star is the product of the four σ_x operators of the spins on edges adjacent to a single vertex of the lattice. In this way, one obtains two sets of L^2 plaquette and star operators, out of which $L^2 - 1$ in each set are independent. Note that these operators can only have eigenvalues $+1$ and -1.

 ©2012 American Physical Society

One can then define a subspace $\mathcal{C}$ of the total Hilbert space given by the $2^{[2L^2-2(L^2-1)]} = 4$ states which are simultaneous eigenstates of all independent plaquettes and stars with eigenvalue $+1$. This space can thus accommodate two logical qubits, and measuring the plaquette and star operators allows one to gather information about possible spin- and phase-flip errors without disturbing the encoded state. A negative plaquette (star) indicates the presence of one or three σ_x (σ_z) spin errors. The toric code belongs to the class of stabilizer codes, and the plaquettes and stars are in that context often referred to simply as stabilizer operators.

Notably, the code space $\mathcal{C}$ is the degenerate ground space of the Hamiltonian

$$H = -J \sum_s A_s - J \sum_p B_p. \tag{1}$$

Here, $J > 0$ is the energy gap, and A_s and B_p are the stars and plaquettes, respectively, explicitly given by

$$A_s = \prod_{i \in \mathrm{adj}(s)} \sigma_x^i, \tag{2}$$

$$B_p = \prod_{i \in \mathrm{adj}(p)} \sigma_z^i, \tag{3}$$

where adj(s) [adj(p)] denotes the set of spins on edges adjacent to the star (plaquette) s (p). The elementary excitations of the Hamiltonian Eq. (1) are stabilizer operators with negative eigenvalue and are referred to as "anyons."

Associated with the two logical qubits encoded in $\mathcal{C}$ are four stringlike operators (products of single-spin σ_x's or σ_z's) which wrap around the torus and commute with all plaquettes and stars, but act nontrivially in the form of logical Pauli X and Z operators on the two qubits encoded in $\mathcal{C}$. We choose to label the operators such that X_1 is a vertical string on horizontal edges and Z_1 is a horizontal string on horizontal edges. Correspondingly, X_2 and Z_2 are horizontal and vertical strings, respectively, on vertical edges [see Fig. 1(a)].

When the system described by the Hamiltonian Eq. (1) is coupled to a noisy environment causing single-spin errors, pairs of anyons are created and can subsequently move diffusively on the toric surface. Eventually, the creation and diffusion of anyons leads to a pattern of errors containing undetectable loops around the torus, acting as unnoticed logical Pauli operators on the code space $\mathcal{C}$ and therefore corrupting the state contained therein. Measurement of the plaquette and star operators to locate anyons reveals some, but not all, information about the underlying error pattern and is generally ambiguous. It is up to an error-correction procedure (see Sec. III B) to deal with this problem in a satisfactory way.

The toric code has gained attention due to a series of interesting and advantageous properties. Namely, the stabilizer operators are local and independent of the system size L, while the code distance grows linearly with L. Closely related is the fact that the ground-state degeneracy is exponentially protected (in L) against local perturbations. Quite remarkably, the toric code is in a sense almost optimal within the class of all CSS codes [5], even though the latter contains codes with arbitrarily large stabilizer operators. We will reconsider this topic in greater detail in Sec. IV C.

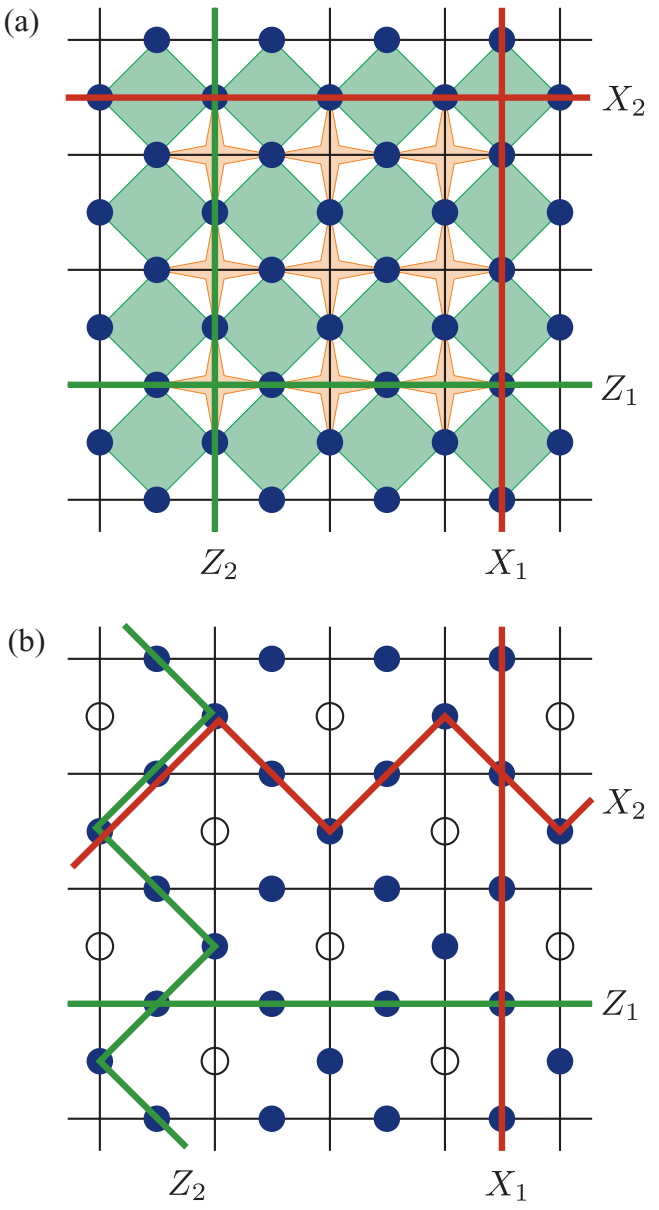

FIG. 1. (Color online) Toric codes. (a) Kitaev's original 2D toric code. Shown is a 4×4 subregion of the $L \times L$ lattice. The blue solid dots on the edges of the lattice represent spins, the four-body plaquette and star operators are shown in light green and orange, respectively (note that stabilizers containing spins outside the figure are not shown). All four logical Pauli operator strings are displayed as thick horizontal and vertical lines. (b) The same region after modifying the lattice in order to incorporate randomness. The modified plaquette and star operators are not shown yet; see Fig. 2. The empty circles indicate the defect positions, i.e., the edges of the lattice where spins are removed. This requires altering the logical operators Z_2 and X_2 in the way shown. Note that all commutation relations between the logical operators are preserved.

III. CLASSICAL DYNAMICS AND NUMERICAL SIMULATIONS

A. Classical dynamics from single-spin errors

Since the Hamiltonian Eq. (1) does not couple the star and plaquette operators, we can treat the two corresponding types

of anyonic excitations independently. Furthermore, because the stars are simply plaquettes on the dual lattice, it is sufficient to study the dynamics of only one type, e.g., the plaquette anyons. We assume that each spin is coupled to an auxiliary system that can cause the spin to flip via σ_x errors. In the limit of weak coupling [17,18], one can derive the following system of coupled rate equations describing the classical dynamics of the system [9]:

$$\frac{d}{dt}p_{\mathcal{E}}(t) = \sum_i \left[\gamma_{i,\mathcal{E}}^{\text{in}}\ p_{x_i(\mathcal{E})}(t) - \gamma_{i,\mathcal{E}}^{\text{out}}\ p_{\mathcal{E}}(t)\right]. \tag{4}$$

Here, $p_{\mathcal{E}}(t)$ is the time-dependent probability of finding the system in the state $|\mathcal{E}\rangle$ obtained by applying σ_x errors to all spins with indices in $\mathcal{E}$, i.e., $|\mathcal{E}\rangle = \prod_{k\in\mathcal{E}} \sigma_x^k |\psi_0\rangle$, where $|\psi_0\rangle$ is the initial state of the system. Similarly, $p_{x_i(\mathcal{E})}(t)$ describes the probability of being in the state $\sigma_x^i|\mathcal{E}\rangle$. Finally, $\gamma_{i,\mathcal{E}}^{\text{in}}$ and $\gamma_{i,\mathcal{E}}^{\text{out}}$ are the transition rates to arrive at or leave the state $|\mathcal{E}\rangle$, respectively, via a σ_x error at the spin with index i.

In this work, we will consider two types of error environment. The first one is a constant-error-rate model, i.e., we set $\gamma_{i,\mathcal{E}}^{\text{in}} = \gamma_{i,\mathcal{E}}^{\text{out}} = \text{const}$. In this case, spin flips are caused independently of any previously existing anyons and σ_x errors. The second model mimics the coupling to a thermal environment, where the transition rates are in general energy dependent. Consequently, we set $\gamma_{i,\mathcal{E}}^{\text{in}} = \gamma(-\omega_{i,\mathcal{E}})$ and $\gamma_{i,\mathcal{E}}^{\text{out}} = \gamma(\omega_{i,\mathcal{E}})$, where $\omega_{i,\mathcal{E}} = \epsilon_{\mathcal{E}} - \epsilon_{x_i(\mathcal{E})}$ is the energy difference between the states $|\mathcal{E}\rangle$ and $\sigma_x^i|\mathcal{E}\rangle$. An expression for $\gamma(\omega)$ often found in the literature is given by

$$\gamma(\omega) = 2\kappa_n \left|\frac{\omega^n}{1-e^{-\beta\omega}}\right| e^{-|\omega|/\omega_c} \tag{5}$$

and can be derived from a spin-boson model [19,20]. Here, κ_n is a constant with units $1/(\text{energy})^n$ setting the time scale, $\beta = 1/k_BT$, with T being the temperature of the bath and k_B denoting Boltzmann's constant, and ω_c is the cutoff frequency of the bath. In the following, we set $\omega_c \to \infty$ for simplicity. A bath with $n = 1$ is called "Ohmic," whereas one with $n \geqslant 2$ is called "super-Ohmic." Only the former case is considered in this work. Unless otherwise stated, all energies will be expressed in units of k_BT. Consequently, the unit of time is $(\kappa_1 k_B T)^{-1}$.

B. Simulations and error correction

Clearly, it is impossible to solve Eq. (4) analytically for meaningful system sizes, because the number of states $p_{\mathcal{E}}$ grows exponentially with L^2. We thus have to stochastically simulate the system and obtain the quantities of interest, such as the number of anyons or the expectation values of the logical operators, by averaging over many (typically several thousand) instances.

In greater detail, the iteration of the simulation at time t consists of these steps: (i) Calculate all unnormalized single-spin-flip probabilities $p_i = \gamma(\epsilon_{\mathcal{E}} - \epsilon_{x_i(\mathcal{E})})$, and then obtain from them the total spin-flip rate $R = \sum_i p_i$. (ii) Draw the time Δt until the next spin flip from an exponential distribution with rate R. (iii) Calculate and record all quantities of interest for time sampling points lying in the interval $[t, t+\Delta t]$. Namely, these quantities are the number of anyons, the number of σ_x errors, and the uncorrected and error-corrected (see below) logical operators Z_1 and Z_2. (iv) Determine a random spin according to the probabilities p_i/R, flip it, and set t to $t+\Delta t$.

The error-correction step in the toric code consists of pairing up all detected anyons and then annihilating them by connecting each pair with a string of errors from one partner to the other. The pairing is usually chosen such that all anyons are annihilated with the smallest total number of single-spin operators. This is known as the minimal-weight perfect matching and can be found in polynomial time with the help of the "blossom" algorithm due to Edmonds [21]. The run-time complexity of this algorithm has been improved several times since its discovery. We are employing the library BLOSSOM V [22] which implements the latest version running in $O(mn\log n)$ time, where n is the number of anyons (vertices) and m the number of connections (edges) between them.

In order to find the true matching with minimal weight, one in principle would need to choose the set of edges to include all connections from every anyon to every other. However, since the size of this set grows quadratically with the number of anyons n, the overall scaling of the matching algorithm becomes $O(n^3\log n)$, which is not feasible for large n. We therefore first perform a Delaunay triangulation in negligible $O(n\log n)$ time using the library TRIANGLE [23]. The result is that only anyons close to each other are connected using a number of edges linear in the number of anyons. It turns out that this is an excellent approximation, yielding results that are nearly indistinguishable from those obtained from a matching over the complete graph.

Within the paradigm of active error correction, where the anyons are detected and corrected periodically on sufficiently small time intervals, the encoded state can be kept free of logical errors almost indefinitely. However, since we are interested in the use of the toric code as a passive quantum memory, we are mostly concerned with the lifetime τ of the encoded information in a scenario where error correction is performed only once at readout. Hence, whenever we show plots of the "error-corrected" logical operators decaying as a function of time, we thereby refer to their values if error correction had been performed at that time, without actually performing it. We then define the lifetime of the system as the time it takes for the expectation values of the error-corrected logical operators to decay to 90% of their initial value.

IV. RANDOM LATTICES

In this section, we study the error thresholds of a family of models obtained by randomly modifying the toric code in a way that preserves its basic features. We first describe how we create our random lattices and then present and discuss the results of the simulations within the context of optimal quantum codes.

A. Generating the lattices

Starting from the toric code on an $L\times L$ lattice, we remove $\frac{1}{2}L^2$ spins at specific and regularly distributed "defect" locations. The structure of the defect pattern can be easily understood from Fig. 1(b). Basically, every second vertical edge is labeled a defect, with the first defect of each row

alternately being created on the first or second vertical edge of that row. Note that the height and width of the grid both must be even in order for this procedure to be consistent with the periodic boundary conditions. We now have to modify all plaquettes and stars as well as the logical Pauli X and Z operators such that all original commutation relations remain unaltered.

Let us start with the logical operators. Clearly, both X_1 and Z_1 (with single-spin operators exclusively on horizontal edges) are unaffected by the introduction of defects on vertical edges of the lattice. However, the pair of operators in the original code acting on the second encoded qubit is defined on vertical edges and thus needs to be adapted. Clearly, the operators must remain connected strings wrapping around both dimensions of the torus. The zigzag pattern shown in Fig. 1(b) achieves this with the smallest increase in the number of single-spin operators. It is straightforward to verify that these new X_2 and Z_2 operators, together with the unaltered pair acting on the first encoded qubit, indeed mutually fulfill all original commutation relations.

We now discuss the modification of the plaquette and star operators. Removal of one spin, i.e., creation of one defect, affects exactly two adjacent plaquettes and two adjacent stars. We will consider two possible ways of dealing with this situation (see Fig. 2). We can either (i) define two restricted three-body plaquettes and one "vertical star" consisting of the product of the remaining six single-spin σ_x operators, or (ii) perform the dual operation, namely, defining one large six-body "horizontal plaquette" and two restricted three-body stars. The two ways of modifying the original operators are depicted in Fig. 2(a). It is relatively easy to see that these new three-body and six-body operators remain mutually commuting and furthermore commute with all modified logical Pauli operators just as in the original code. Note that also the dimension of the code space is left unchanged since it generally only depends on the genus of the surface covered by the anyon operators [4]. We can now create a random lattice by choosing at each defect site to create a six-body plaquette with probability p_{mix} and two three-body plaquettes with probability $1 - p_{\text{mix}}$. See Fig. 2(b) for a typical example. The special case $p_{\text{mix}} = 0$ corresponds to a regular lattice of three-body plaquettes and six-body stars, whereas $p_{\text{mix}} = 1$ conversely yields a regular lattice of six-body plaquettes and three-body stars. In both cases, the three-body operators are the vertices of an underlying hexagonal lattice, whereas the six-body operators form the vertices of its dual, the triangular lattice.

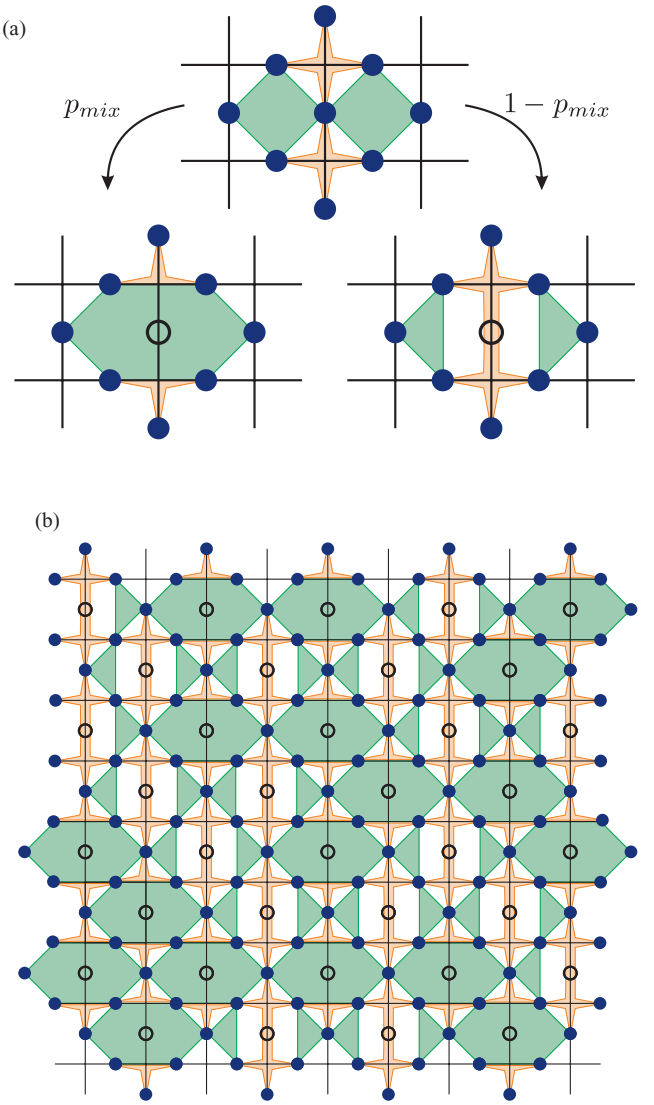

FIG. 2. (Color online) Modifying the stabilizer operators. (a) When removing a spin (empty circle), we choose between two ways of adapting the affected stabilizer operators. With probability p_{mix} we join the two plaquette operators to one large six-body operator and reduce the two stars from four- to three-body operators. Alternatively, with probability $1 - p_{\text{mix}}$, we perform the dual operation, namely, we define two three-body plaquettes and one large six-body star. Spins and operators not affected by removing the central spin are not shown in this example. (b) Typical 8×8 subregion of a (larger) random lattice with $p_{\text{mix}} = 0.5$. Logical operators as well as some spins and operators at the edges with the rest of the lattice are not shown.

B. Results

Before we start discussing the results, we would like to briefly point out a modification to the error-correction scheme we had to incorporate in order to deal with the random lattices. Since it would be difficult to adapt the Delauny triangulation to an irregular graph, we have replaced this step by a breadth-first search performed on each anyon. This procedure connects every anyon to at most k of its nearest neighbors, where distance is measured not in a Euclidean sense, but as the number of errors in a connecting string. For constant k, this requires a run time of $O(n)$, where n is the number of anyons. We have found that $k = 10$ is an excellent approximation to $k = \infty$ and have used this value in all calculations.

We have performed a series of Monte Carlo simulations to determine the critical fraction of errors f_{cr}^{Z} independent of any form of anyon dynamics (see Appendix A for additional results in the case of thermal errors). If the probability for each spin to independently be affected by a σ_x error becomes larger than this critical value in the limit $L \to \infty$, the error-correction scheme undergoes a transition from performing fully accurate

error recovery to randomly guessing the error-corrected state with the lowest possible success rate of 50%. We can determine f_{cr}^{Z} by plotting the expectation values of the error-corrected logical Z operators as a function of the error probability f for different lattice sizes and observe at which value of f the curves intersect [24].

Figure 3(a) displays typical results for a few different values of p_{mix}. We observe that the expectation values of Z_1 and Z_2 in general have a different dependence on the error probability f. This is due to the fact that on a lattice with, e.g., a majority of six-body plaquettes, it takes on average fewer spins to form a loop around the horizontal direction of the torus than around the vertical one. The opposite argument holds in the case of a three-body plaquette majority. Not surprisingly, Z_1 and Z_2 decay identically for a 50% mixing of three- and six-body plaquettes. Note that, despite the typically unequal decays of Z_1 and Z_2 as a function of f, the error thresholds for the two operators are always identical for a given value of p_{mix}. This is consistent with the general understanding that the correctability of the memory as a whole is related to the phase of a corresponding random-bond Ising model [5]. Indeed, our numerically determined thresholds for the regular three-body and six-body plaquette lattices agree well with the recently calculated multicritical points in spin-glass models on hexagonal and triangular lattices, respectively [25]. Specifically, we find $f_c \approx 0.1585$ for $p_{\mathrm{mix}} = 0$ (theoretical value: $f_c = 0.1640$) and $f_c \approx 0.0645$ for $p_{\mathrm{mix}} = 1$ (theoretical value: $f_c = 0.0674$). The discrepancy of about 4%-5% between the numerical and theoretical thresholds is of the same size as in the case of the toric code on a square lattice (where we found $f_c \approx 0.1055$ as compared to the theoretical value $f_c = 0.1092$) [9] and can generically be attributed to the failure of the minimal-weight perfect matching close to the threshold. Interestingly, our numerical results suggest that the thresholds of the toric code and our random lattice models with $p_{\mathrm{mix}} = 0.5$ are identical.

We show in Fig. 3(b) the critical fraction of errors f_{cr}^{Z} for the logical Z operators determined in the way described above as a function of the lattice mixing probability p_{mix}. Since the plaquette and star lattices are dual to each other (to every six-body plaquette correspond two three-body stars, and vice versa), the critical fraction f_{cr}^{X} of σ_z errors for which error correction of the logical X operators fails [also plotted in Fig. 3(b)] is simply given by

$$f_{cr}^{X}(p_{\mathrm{mix}}) = f_{cr}^{Z}(1 - p_{\mathrm{mix}}). \tag{6}$$

At equal mixing, i.e., $p_{\mathrm{mix}} = 0.5$, the threshold values are given by $f_{cr}^{X}(0.5) = f_{cr}^{Z}(0.5) \approx 0.1055$.

Consequently, one of the thresholds for the two different types of Pauli operators is that either f_{cr}^{X} or f_{cr}^{Z} is always smaller than or equal to the threshold of the toric code. Our random lattices thus bear no advantage over the latter in the case of a uniform-error model, where σ_x and σ_z errors occur with the same probability. The situation is different, however, for biased noise. If bit flips and phase flips are created with different probabilities, we can make use of the asymmetry in the error thresholds for $p_{\mathrm{mix}} \neq 0.5$. Assuming, for instance, that σ_x errors are more frequent than σ_z errors would lead to an overall lifetime decrease of encoded states in the toric code due to the shorter lifetimes of the logical Z operators. However,

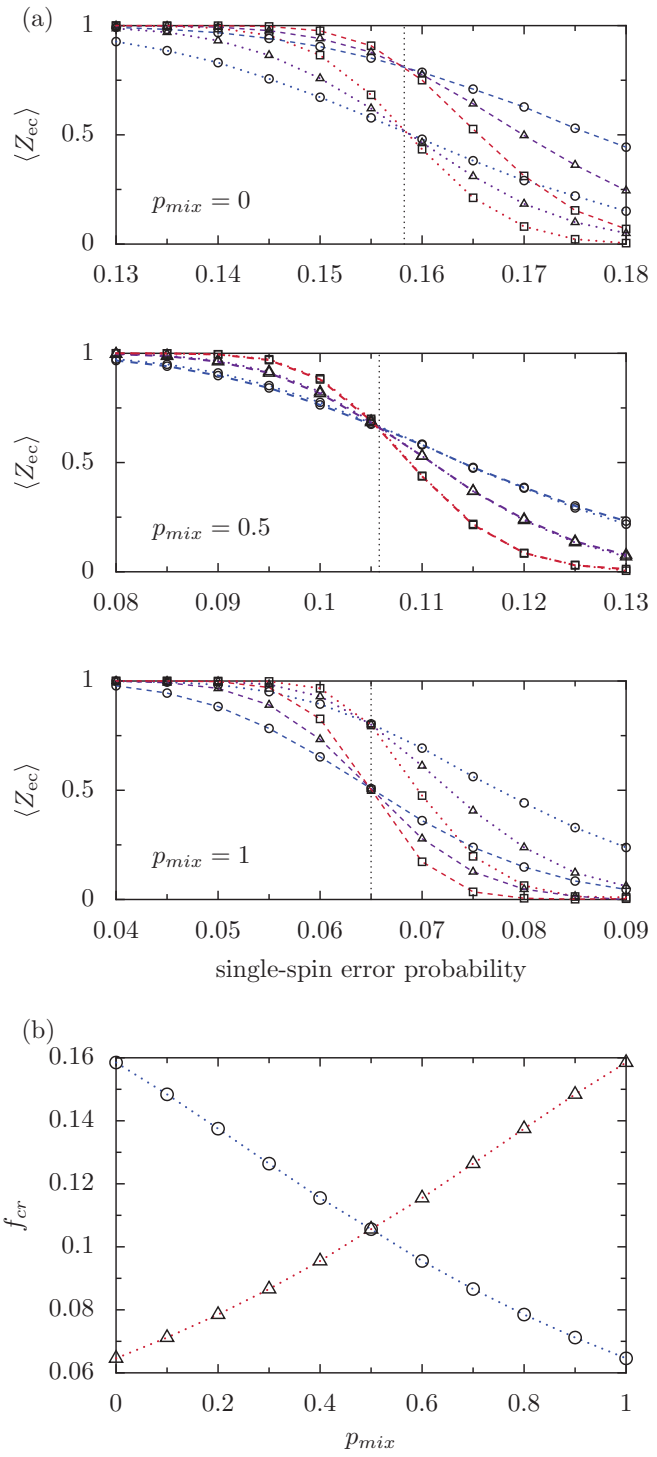

FIG. 3. (Color online) Critical error thresholds of random models. (a) Three example plots of data used to determine the critical error thresholds. Each plot shows, for a specific value of p_{mix}, the expectation values of the logical Z_1 (dotted lines) and Z_2 (dashed lines) operators for grid sizes $L =$ 32 (circles), 64 (triangles), and 128 (squares). The vertical dotted lines indicate the position of the error threshold. Data points are obtained by bootstrapping 1000 sample values, each of which is obtained by averaging over 200 random error distributions on a single instance of a random lattice. (b) Error thresholds [as determined in (a)] of Z (circles) and X (triangles) operators as a function of p_{mix}. The dotted lines are guides to the eye.

starting from a random model at $p_{\text{mix}} = 0.5$, a decrease in p_{mix} will lead to an increase of the Z lifetimes and a decrease of the X lifetimes. If the error frequencies are not too different, the lifetimes will become identical at some value $0 \leqslant p_{\text{mix}} < 0.5$ and will be larger than the overall lifetime of the toric code. We thus conclude that the random lattices can be employed to increase the lifetime of encoded states compared with the toric code on a square lattice in the presence of biased noise. While these lattices require both error probabilities to fall in the range $0.0674 \leqslant p \leqslant 0.1640$ (and below the boundary in Fig. 4; see the next section), it should in principle be possible to extend this range to $0 \leqslant p \leqslant 0.5$ by defining stabilizers with more than six single-spin operators in a similar fashion.

C. Relation to optimal quantum codes

We now discuss our random lattices within the context of optimal quantum coding. It is well known that, assuming a biased-constant-error model, there is an upper bound on the fraction of logical qubits k and physical qubits n that encode them, valid for all CSS codes. This bound is given by Refs. [5,16,26]

$$k/n \leqslant 1 - H(p_x) - H(p_z), \tag{7}$$

where $H(x) = -x \log_2 x - (1-x)\log_2(1-x)$ is the Shannon entropy, and p_x and p_z are the probabilities for a single spin to be affected by a σ_x and a σ_z error, respectively. The bound Eq. (7) can be motivated with the following intuitive (but somewhat hand-waving) argument we were not able to find in the literature.

An ideal CSS code would be able to detect for each physical qubit if it was suffering from a σ_x or a σ_z error. Assuming that these errors are uncorrelated, the number of classical bits required to store this information is asymptotically given by $nH(p_x) + nH(p_z)$. If we are to store the same information in qubits instead of bits, the Holevo bound [1] requires the usage of at least as many qubits to do so. Since our optimal CSS code needs to store the information of k encoded qubits, as well as all possible occurrences of errors, we have

$$n \geqslant k + nH(p_x) + nH(p_z). \tag{8}$$

Division by n and rearrangement of terms yields the desired bound Eq. (7).

For unbiased errors with $p = p_x = p_z$, the right-hand side of Eq. (7) becomes zero at $p \approx 0.110\,028$, implying that there cannot be any CSS code coping with an error rate larger than this value. Quite remarkably, the critical error probability for the toric code has been determined to be $f_{cr} = 0.109\,187$ [25]. This is astonishingly close to the upper bound, especially when taking into account that all stabilizers are local four-body operators. Moreover, insertion of the error thresholds for the regular six-body plaquette lattice and its dual lattice of three-body stars ($p_{\text{mix}} = 1$) into the right-hand side of Eq. (7) gives

$$1 - H(0.0674) - H(0.1640) \approx 6 \times 10^{-5}, \tag{9}$$

which is virtually zero, indicating that the code is close to optimal for this particular biased-error model. Due to the symmetry of Eq. (7) with respect to the error probabilities and the duality of the triangular and hexagonal lattices, the same argument holds for a lattice with three-body plaquettes and six-body stars ($p_{\text{mix}} = 0$) with the values of p_x and p_z exchanged. With our random lattices, we can thus continuously interpolate between two optimal models by changing p_{mix}. This suggests that the random models are optimal for all values of p_{mix}, in the sense that for every $0.0674 \leqslant p_x \leqslant 0.1640$ there is a random model with a theoretically (close to) maximal possible threshold for p_z. The results plotted in Fig. 4 strongly support this claim. The solid line is the zero contour of the upper bound Eq. (7) and the crosses are the threshold pairs of the random lattices determined numerically. Note that the numerical data are within the typical 5% distance of the theoretical bound. This can once again be explained by the failure of the minimal-weight error-correction algorithm close to the thresholds. This observation, together with the knowledge from theory that the models are virtually optimal for $p_{\text{mix}} = 0$ and $p_{\text{mix}} = 1$, leads us to conjecture that the random models are virtually optimal for all values of p_{mix}. However, to carry out a theoretical study in the fashion of Ref. [25] is outside of the scope of the present work and is deferred for future research.

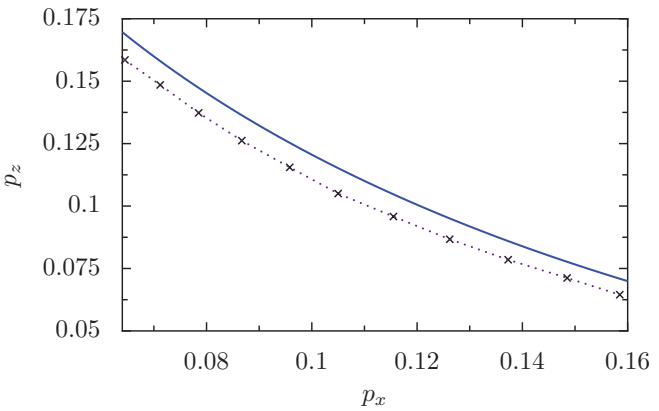

FIG. 4. (Color online) Theoretical upper bound on biased noise correctable by CSS codes. Given an error model of independent σ_x and σ_z errors occurring with constant probabilities p_x and p_z, respectively, there exists no CSS code able to cope with pairs of error probabilities lying above the solid line given by the zero contour of Eq. (7). The crosses are the numerically determined pairs of thresholds of the random models for $p_{\text{mix}} = 1$ down to $p_{\text{mix}} = 0$ from left to right. The dotted line is a guide to the eye.

V. RANDOM ON-SITE POTENTIALS

This section is devoted to the study of the classical dynamics of anyons in the regular toric code on a square lattice, but with randomly modified anyon on-site energies. We are also particularly interested in the case where long-range anyon-anyon interaction is present, as this has been shown to generally enhance the lifetime of the memory due to the suppression of the anyon density with increasing system size [9]. For this, it is convenient to introduce the modified stabilizer operators $n_s = (1 - A_s)/2$ and $n_p = (1 - B_p)/2$, where A_s and B_p are the usual star and plaquette operators, respectively. These operators are zero in the absence of an anyon on the respective

site and equal to 1 otherwise. The more general Hamiltonian can then be written as

$$H = \frac{1}{2}\sum_{pp'} U_{pp'} n_p n_{p'} + \frac{1}{2}\sum_{ss'} V_{ss'} n_s n_{s'}, \tag{10}$$

where $U_{pp'}$ and $V_{ss'}$ contain the on-site energy and repulsive anyon interaction terms. Since in this model plaquette and star anyons are still independent, we can set $V_{ss'} = 0$ and note again that all results for the plaquette anyons hold equally for the stars. We then set

$$U_{pp'} = 2J_p\delta_{pp'} + \frac{A}{(r_{pp'})^\alpha}(1-\delta_{pp'}), \tag{11}$$

where J_p is the on-site energy of an anyon on the plaquette with index p, A is the interaction strength, $r_{pp'}$ is the shortest distance on the torus between plaquettes p and p', and $0 \leqslant \alpha < 2$ is the (long-range) interaction exponent. The on-site energies J_p are chosen randomly from a distribution with mean zero in order to discriminate effects caused by the randomness from those potentially caused by the system having a nonzero mean gap.

We focus on the case of constant interaction, i.e., $\alpha = 0$, and Ising-like randomness, meaning that the J_p are chosen from $\{-\sigma, +\sigma\}$ with equal probabilities. We refer to $\sigma \geqslant 0$ as the disorder strength. This model is interesting mostly for two reasons. First, it is the most convenient system incorporating randomness with respect to numerical simulation. Since the interaction is constant and thus simply depends on the total number of anyons, only six different single-spin-flip rates need to be updated at each iteration step, depending on the number and configuration of adjacent anyons and on-site energies, respectively. Second, this simple model already displays all dynamical effects also present in more complicated systems (e.g., $\alpha \neq 0$ and a Gaussian distribution of J_p's; see Appendix B) and thus serves as an ideal playground for studying and understanding these effects. Naively, one would expect that the presence of negative on-site energies in the system simply favors the creation of anyons and is thus always disadvantageous for the lifetime of the memory. While this is indeed true for a noninteracting system, we find a regime in the interacting case where, quite surprisingly, the lifetime is enhanced for increasing disorder strength.

Figure 5 presents the results for the two cases. The noninteracting system is stable against disorder strengths that are roughly equal to the temperature but then decays for larger σ. This can be understood easily from the detailed balance condition satisfied by the rates Eq. (5): The ratio of the creation and annihilation rates of a pair of anyons on two sites with negative on-site energy is given by $\gamma(2\sigma)/\gamma(-2\sigma) = \exp(2\beta\sigma)$, which becomes large for σ's exceeding the temperature. It is thus exponentially more likely for a pair of anyons to be created than annihilated for $\sigma > k_BT$, thereby quickly cluttering the system with anyons and crossing the critical fraction of errors. This situation changes completely in the presence of interactions between the anyons. The data shown in Fig. 5 display a steep increase in the lifetime as a function of the disorder strength, peaking at around $\sigma \approx 3.5 k_BT$ for that particular system, followed by a slower decay.

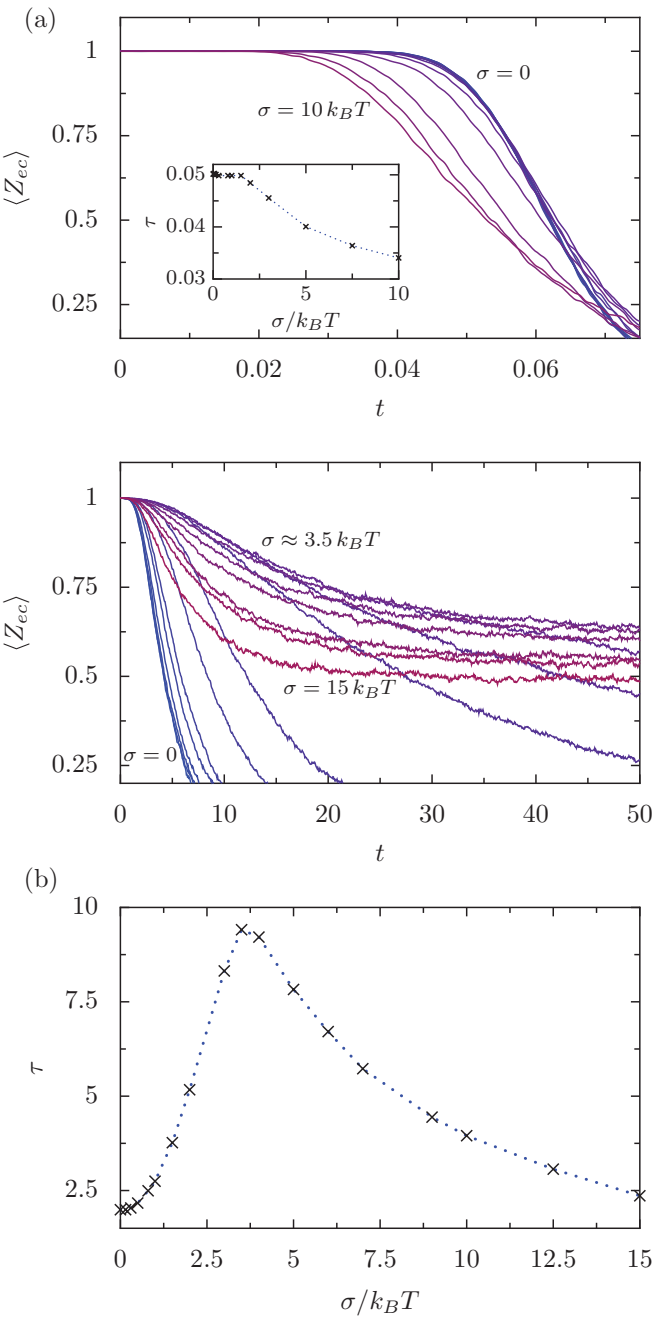

FIG. 5. (Color online) Influence of disorder on the memory lifetime. (a) Time evolution of error-corrected Z operators for a noninteracting (top) and interacting (bottom, $\alpha = 0$, $A = 0.5$) model. Both systems are of size 32×32 unit cells (2×32^2 spins) and are coupled to an Ohmic bath at temperature $T = 1$. The different curves display $\langle Z_{ec}(t)\rangle$ for different disorder strengths σ of Ising-like randomness with on-site energies $J_p = \pm\sigma$. In the noninteracting system, σ is increased from 0 to $10k_BT$ as indicated in the panel. The inset displays the lifetime of the memory, i.e., the time at which $\langle Z_{ec}\rangle$ hits 0.9, as a function of σ. The disorder strengths examined in the interacting case have been chosen as $0 \leqslant \sigma \leqslant 15k_BT$ (see main text and labels in the panel). (b) The lifetimes of the interacting model extracted from the curves of the lower panel in (a). The dotted line is a guide to the eye.

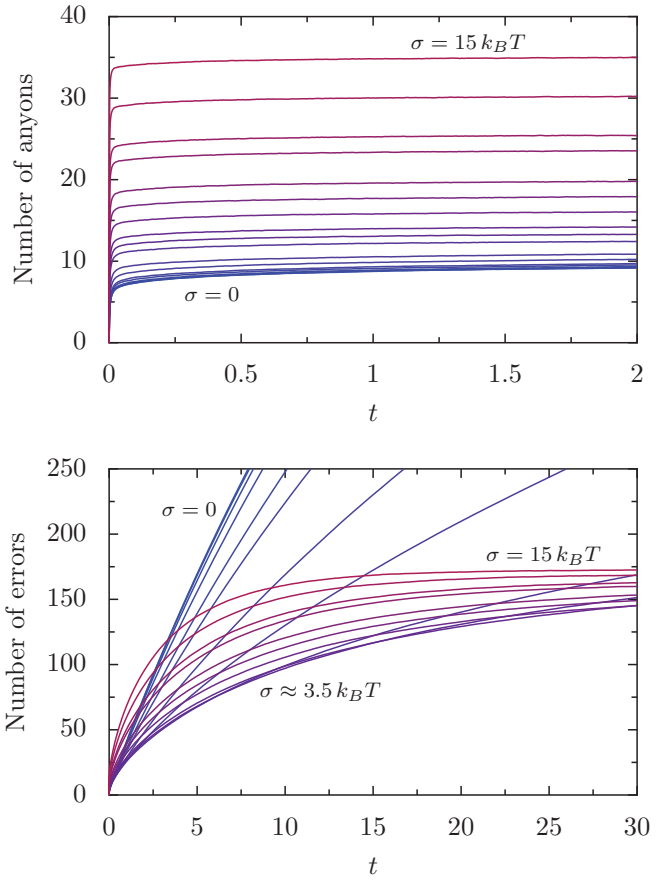

FIG. 6. (Color online) Number of anyons (top) and number of single-spin errors (bottom) as a function of time in an interacting system ($\alpha = 0, A = 0.5k_BT$) of size 32×32 coupled to an Ohmic bath. The strength of the Ising-like randomness is increased from $\sigma = 0$ to $\sigma = 15k_BT$ as indicated in the panels (see also main text).

We can shed some light on this effect by additionally looking at the number of anyons and the number of errors as shown in Fig. 6. For any fixed value of σ, the number of anyons again increases quickly but then saturates almost instantaneously at the equilibrium value. At this point, creating a new pair of anyons costs an energy penalty due to the repulsive interaction that can no longer be compensated by the negative on-site potentials. One can clearly see that the equilibrium number of anyons increases linearly with σ, which implies that the corresponding enhanced memory lifetimes cannot be explained by a suppression of the anyon density.

However, the error creation rate (i.e., the slope of the curves in the lower panel of Fig. 6) exhibits a pronounced minimum at the same value $\sigma \approx 3.5k_BT$ that also yields the maximal lifetime. Such an initial decrease in the error rate despite an increasing number of anyons can only be consistently explained by a suppression of the anyon diffusion.

For disorder strengths $\sigma \gg k_BT$, processes that create anyons on two positive sites or that move an anyon from a negative to a positive site are exponentially suppressed. The positive sites thus effectively act as infinite barriers that greatly reduce the mobility of the anyons, and the encoded state is solely destroyed by diffusing anyons restricted to the negative sites [27]. As the disorder strength is lowered, two competing effects come into play. On the one hand, the number of anyons is reduced linearly. On its own, this would lead to a longer lifetime due to the presence of fewer diffusing anyons. On the other hand, the barriers separating the regions of negative sites are lowered, which facilitates the diffusion across longer distances and promotes a reduction in lifetime. The observed maximum in the memory lifetime can thus be understood as a tradeoff between having few but relatively freely moving anyons for $\sigma \ll k_BT$ and more but very restricted anyons for $\sigma \gg k_BT$. The interaction merely plays the role of restricting the anyons to a small enough (for $\sigma \lesssim k_BT$) and constant number. Appendix C contains results that further support the picture described above.

VI. QUANTUM DYNAMICS

The toric code ground state has been shown to be stable against local perturbations of sufficiently small strength [28,29]. The effect on exited states, however, is more disastrous. Perturbations allow the hopping of any anyons that are present, causing the quantum memory to become unstable [30,31]. It has been found that this problem can be solved by the presence of disorder in the couplings of the model [12,13], since the disorder suppresses anyon motion through a localization effect. In this section we study the effects of the disorder introduced by using the random lattices.

A. Error model

Consider the toric code Hamiltonian, perturbed by a magnetic field of strength h. For concreteness, let us choose this to be of the form

$$H = \sum_p J_p n_p + \sum_s J_s n_s + h \sum_i \sigma_x^i. \tag{12}$$

The effects of such a perturbation have been studied using the methods of Refs. [12,13], where it was noted that, since the σ_x^i do not commute with the n_p, the perturbation will have the effect of creating, annihilating, and transporting plaquette anyons. For $h \ll J_p$ all these effects apart from the transport are suppressed by the energy gap, allowing the system to be modeled as the following many-particle quantum walk Hamiltonian:

$$H_p = \sum_{p,p'} M_{p,p'} t_{p,p'} + U \sum_p n_p(n_p - 1),$$
$$M_{p,p'} = \delta_{\langle p,p'\rangle} h + \delta_{p,p'} J_p. \tag{13}$$

Here $\delta_{\langle p,p'\rangle} = 1$ only when the plaquettes p and p' share a spin. The operator $t_{p,p'}$ maps a state with an anyon on the plaquette p to that with the anyon moved to p', and annihilates any state without an anyon initially on p. Since the anyons are hard-core bosons, we are interested in the case of $U \to \infty$.

This effective description in terms of quantum walks of anyons holds also for a more general magnetic field and other local perturbations. The effects of anyonic braiding occur at a higher order of perturbation theory than those of this effective description, and hence may be ignored. The dynamics of the plaquette and vertex anyons can therefore be considered separately. Since they are dual to each other, once again only

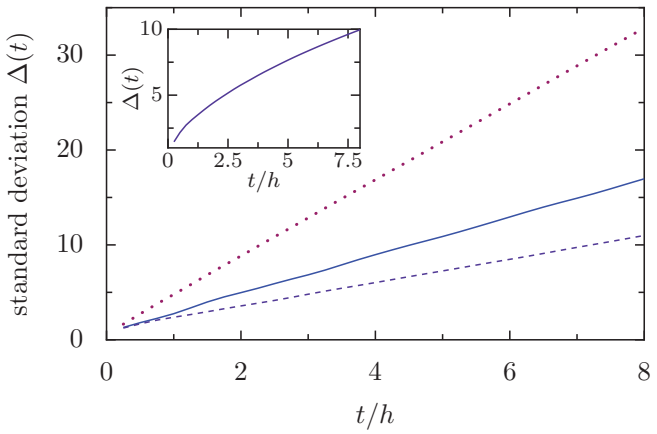

FIG. 7. (Color online) Time evolution of the standard deviation $\Delta(t)$ of a single quantum walker on lattices with uniform couplings $J_p = J$ for all p. The different curves correspond to a square lattice (solid), three-body plaquette lattice (dashed), and six-body plaquette lattice (dotted). Inset: $\Delta(t)$ on the random lattices from Sec. IV with $p_{\text{mix}} = 0.5$, where each point has been averaged over 1000 samples.

the plaquette anyons are considered here, without loss of generality.

The Hamiltonian H_p is difficult to solve in general. However, note that the dynamics of H_p are driven by the matrix M, i.e., the Hamiltonian for a single-particle walk. Hence, by considering the case of a single anyon, important aspects of the behavior for the many-particle walks can be determined. It is this approach that is taken here. The Hamiltonian M is applied to a single anyon, initially placed on an arbitrary plaquette of the code. The motion of the anyon can be characterized by the time evolution of its standard deviation Δ. Since finite values of the system size L must be used in the numerics, the walks will, at some point, interact with the boundary. In order for this effect to be ignored, the run time of the walks is limited to ensure that this interference always remains negligible.

The behavior of Δ over time for walks on square, triangular, and hexagonal lattices for which all J_p are uniform can be found in Fig. 7. In each case the standard deviation of the distance increases linearly with time, demonstrating the ballistic motion expected from quantum walks when no disorder is present.

The ballistic motion caused by the field is highly damaging to the quantum information stored within the code. Suppose that the toric code initially has some density ρ of anyon pairs, due perhaps to noisy preparation of the state or interaction with the environment. If ρ is sufficiently small then the pairs will be far apart, allowing error correction to be performed reliably. However, when the perturbation is present this will remain true only for a finite lifetime τ, after which the motion of the anyons prevents them from being paired reliably. This occurs when they have moved a distance comparable to the average distance between pairs, and hence when $\Delta(\tau) \sim 1/\sqrt{\rho}$. Since $\Delta(t)$ grows linearly with time for ordered quantum walks (see Fig. 7), the quantum memory will fail within a time of order $\tau = O(1/\sqrt{\rho})$. Mechanisms which slow down the anyons are therefore favorable to the quantum memory, since they lead to longer lifetimes. It is this effect that is expected from the disorder.

B. Random lattices

Let us now introduce disorder by using the random lattice of Sec. IV while still keeping the J_p (and J_s) uniform, all taking the same value J. Specifically the case of $p_{\text{mix}} = 0.5$ is considered, to maintain the symmetry between plaquette and star anyons. The behavior of the standard deviation of the distance moved by a single walker is shown for this lattice in the inset of Fig. 7. Rather than increasing linearly with time t, as in the ordered case, it is found that $\Delta(t)$ grows with the square root of t. The motion of a quantum walker is therefore diffusive rather than ballistic in this case. As such, the random lattice leads to a significant slowing of the anyon motion, increasing the lifetime to $\tau = O(\rho^{-1})$ (note that we always have $\rho \leqslant 1$). It is possible that the random lattice also induces Anderson localization [32], in which case the lifetime will be increased further, but the system sizes which may be probed are too small for this to be evident.

C. Random lattices together with J disorder

It is known that, when disorder in the J_p couplings is present in the toric code, Anderson localization is induced [12,13]. This effect exponentially suppresses the motion of the walkers, and causes the standard deviation of the distance to converge to a constant value. We therefore have $\tau \to \infty$, i.e., the memory stays stable against the perturbation for an arbitrarily long time. It is now important to determine whether the combination of randomness in both the lattice and the J_p couplings enhances or diminishes this effect.

To study this, disorder in the J_p couplings is considered. Specifically, each J_p randomly takes either the value $J - \sigma$ or $J + \sigma$ with equal probabilities. The value of J is unimportant, but the ratio of σ/h characterizes the strength of the disorder in comparison to the magnetic field. Guided by the numerical results of Ref. [12], we consider here disorder of strength $\sigma/h = 250$ to ensure that the localization effect is observed for moderately sized systems.

In Fig. 8, the time evolution of the standard deviation is shown for the case of J disorder on a square and a random

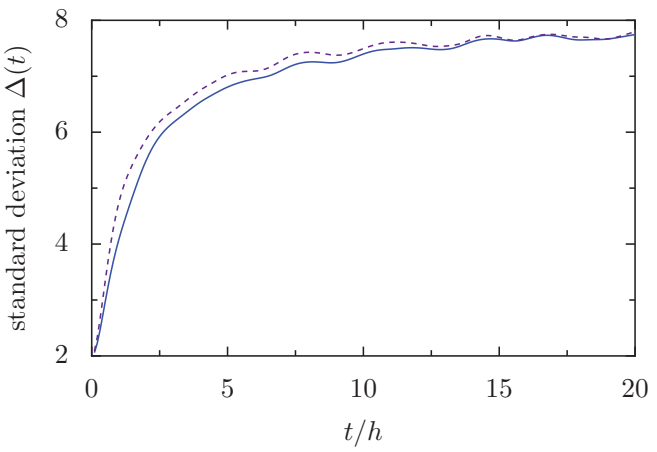

FIG. 8. (Color online) Time evolution of the standard deviation $\Delta(t)$ for a single anyonic walker with disorder in the J_p of $\sigma/h = 250$, on both a square lattice (solid line) and a random lattice (dashed line) with $p_{\text{mix}} = 0.5$. Each point has been averaged over 1000 samples.

lattice. In both cases the localization effect is seen, with the walk unable to move far beyond a few times the length scale separating neighboring vertices. The walks with and without the lattice disorder give very similar results, especially at longer times. The effect of localization in the random lattice therefore seems the same as that of the square, without significantly enhancing or diminishing the effect.

VII. SUMMARY

We have studied the influence of quenched disorder on the incoherent (classical) motion of anyons in modified forms of the toric code. We have first described a class of random models that can be obtained from the toric code by removing a regular sublattice of spins and then for each defect site randomly choosing one of two ways to adapt the affected stabilizers with a probability p_{mix}. The critical fractions of independent errors at which these codes become uncorrectable have then been determined numerically as a function of p_{mix}. We have shown that in the presence of biased noise, where bit flips and phase flips occur at different probabilities, the models based on random lattices can tolerate higher thresholds than the toric code in one type of error, given that the other type is correspondingly lower. These thresholds have been demonstrated to be close to the upper bound correctable by any CSS code. Second, we have studied the toric code subject to randomness in the on-site potentials. Specifically, we have demonstrated that in the presence of repulsive long-range interaction between anyons, there is a pronounced maximum in the lifetime of encoded states as a function of disorder strength. This effect has been attributed to a reduction of anyon diffusion due to the sites with positive on-site energy acting as barriers for the anyons. Finally, the effects of both forms of disorder are studied for coherent transport of the anyons. It is found that the random lattices cause the anyons to move diffusively rather than ballistically, increasing the lifetime of the memory. Adding randomness in the potentials then causes the anyons to localize, leading to further stability.

ACKNOWLEDGMENTS

We would like to thank S. Chesi, K. A. van Hoogdalem, and D. P. DiVincenzo for fruitful discussions. This work was partially supported by the EPSRC, the Royal Society, the Swiss NSF, NCCR Nanoscience Basel, and DARPA.

APPENDIX A: CRITICAL FRACTION OF RANDOM LATTICES IN CONTACT WITH AN OHMIC BATH

We present here some additional results for the error thresholds of random lattices in the presence of thermal errors. Figure 9 shows the fraction of errors f at the lifetime of an infinitely large system as a function of the lattice mixing p_{mix} and for different temperatures T. In this section, the energy scale is set by the anyon gap J. Time is thus measured in units of $(\kappa_1 J)^{-1}$. For given p_{mix} and temperature T, we first simulate systems of several different sizes in contact with an Ohmic bath. We then determine the lifetime τ as the intersection of the decay curves of the corresponding error-corrected logical Z operators (see inset of Fig. 9). Since the anyon dynamics

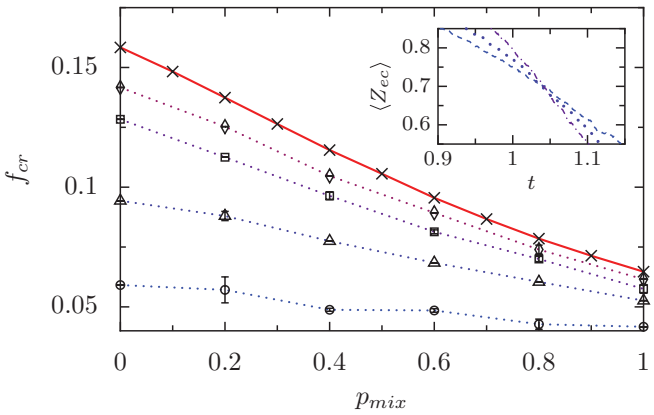

FIG. 9. (Color online) Critical fraction of errors $f_{cr} = f(t = \tau)$ as a function of lattice mixing p_{mix} at temperatures $T = 0.2J$ (circles), $0.45J$ (triangles), $1.0125J$ (squares), and $2J$ (diamonds). The lifetime τ is given by the intersection of error-corrected logical Z operators for lattice sizes $L = 38,56,86$. Error bars are due to the uncertainty in τ. The solid line is determined by the thresholds from the Monte Carlo simulations of an independent-error model (see main text). The inset shows an example of crossing logical Z operators for the particular values $p_{\text{mix}} = 0.4$ and $T = 0.45J$.

are independent of the system size (note that the anyons are not interacting with each other), all curves $f(t)$ for different system sizes collapse and the specific value $f(t = \tau) = f_{cr}$ can be read off easily. One can see nicely that these thresholds converge with increasing temperature to the ones given by the model of independent errors. This can be explained by the loss of correlations between errors due to an increasing amount of thermal noise in the form of fluctuating anyons.

APPENDIX B: GAUSSIAN NOISE AND $1/r$ INTERACTION

We have also performed simulations with $1/r$ interaction ($\alpha = 1$) and plot the results in Fig. 10. Apart from Ising-like disorder ($J_p = \pm\sigma$) we have also looked at a Gaussian distribution of on-site potentials J_p with mean zero and standard deviation σ. Generally, the lifetimes are shorter than for constant interaction because the weaker $1/r$ interaction

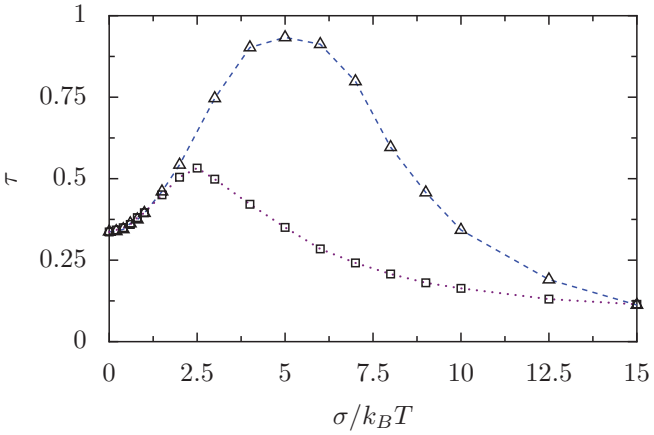

FIG. 10. (Color online) Lifetime τ as a function of disorder strength σ in the presence of Gaussian (triangles) and Ising (squares) noise in an interacting system with $\alpha = 1$, $A = 0.5k_BT$. The lines are guides to the eye. The size of this particular system was $L = 32$.

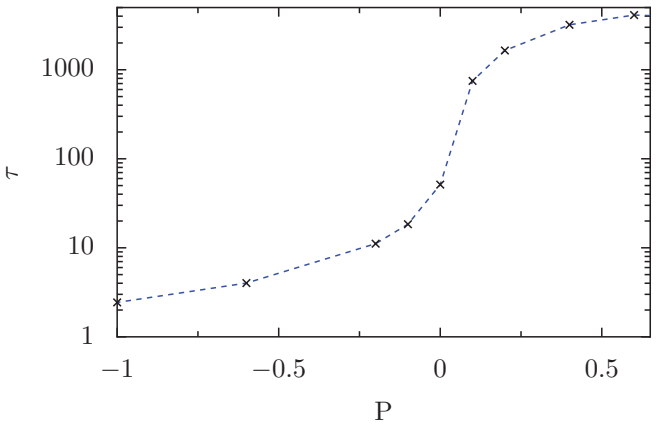

FIG. 11. (Color online) Lifetime as a function of Ising polarization P. The parameters for these systems are $L = 50$, $\alpha = 0$, $A = 0.5k_BT$, $\sigma = 5k_BT$. The dashed line is a guide to the eye.

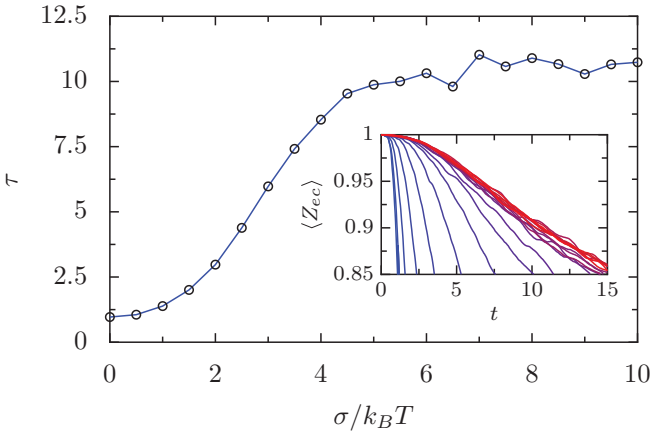

FIG. 12. (Color online) Lifetime as a function of Ising disorder strength in a noninteracting system of size $L = 32$ with an artificially engineered maximal number of anyons equal to 20. The solid line is a guide to the eye. Inset: The error-corrected logical Z operator as a function of time for different σ yielding the lifetimes shown in the main plot.

allows for a larger density of anyons. Nevertheless, the results are qualitatively similar to the ones discussed in the main text, namely, showing a pronounced maximum of the lifetime as a function of σ. This supports the picture that the interaction is required to limit the number of diffusing anyons, while the initial increase in lifetime with σ is due to their obscured diffusion. In the case of Gaussian noise, the latter effect is even stronger, because anyons are created or get trapped in a few sites with on-site potentials much lower than $-\sigma$, out of which it is difficult for them to escape again. This explains the increased lifetime from Ising to Gaussian randomness.

APPENDIX C: SUPPORTING SIMULATIONS

1. Polarized Ising randomness

In order to confirm the picture that it is indeed the sites with $J_p > 0$ that restrict the diffusion by acting as barriers to the anyons, we have determined the lifetime τ of an interacting system ($L = 50, \alpha = 0, A = 0.5\,k_BT, \sigma = 5\,k_BT$) as a function of the Ising polarization P (see Fig. 11). The latter is defined as $P = 1 - 2\eta$, where η is the fraction of sites with negative on-site energy.

Starting from $P = -1$, i.e., $J_p = -\sigma$ for all sites p, the lifetime moderately increases as more and more positive sites are randomly added (increasing P). Around $P = 0$, where there is an equal number of sites with positive and negative on-site energies, the lifetime drastically increases by about two orders of magnitude. At this point, large connected areas of sites with $J_p < 0$ can no longer exist, such that the anyons can move freely only within areas each consisting of just a few negative sites. Consequently, the diffusion is drastically reduced. If and how the polarization at this threshold is related to the site and bond percolation thresholds of the square lattice, which are $\eta \approx 0.5927$ and 0.5 (see, e.g., Ref. [33]), respectively, is not completely clear at the time of writing and remains the subject of future research.

2. Artificial cutoff of number of anyons

We can support the claim that the only relevant effect of the repulsive interaction is to reduce the number of anyons by simulating a noninteracting system with an artificial maximal number of anyons. These data are shown in Fig. 12. Despite the absence of interaction, the lifetime of encoded states is still growing with increasing Ising disorder strength, hence clearly demonstrating that this effect is caused solely by the disorder. Furthermore, the lifetime saturates for large σ, because the energy barriers posed by the sites with $J_p = +\sigma$ are essentially infinitely high and increasing them further bears no more advantage. The observed saturation also confirms that it is indeed the growing number of anyons that is responsible for the subsequent decrease in lifetime at large σ in the data presented in the main text (where the number of anyons was not artificially restricted).

[1] M. A. Nielsen and I. L. Chuang, *Quantum Computation and Quantum Information* (Cambridge University Press, New York, 2000).
[2] N. D. Mermin, *Quantum Computer Science: An Introduction* (Cambridge University Press, Cambridge, 2007).
[3] D. Gottesman, in *Quantum Information Science and Its Contributions to Mathematics*, in *Proceedings of Symposia in Applied Mathematics*, Vol. 68 (AMS, Providence, RI, 2010), p. 13.
[4] A. Y. Kitaev, Ann. Phys. (NY) **303**, 2 (2003).
[5] E. Dennis, A. Kitaev, A. Landahl, and J. Preskill, J. Math. Phys. **43**, 4452 (2002).
[6] D. Bacon, Phys. Rev. A **73**, 012340 (2006).
[7] Z. Nussinov and G. Ortiz, Ann. Phys. (NY) **324**, 977 (2009).
[8] A. Hamma, C. Castelnovo, and C. Chamon, Phys. Rev. B **79**, 245122 (2009).

[9] S. Chesi, B. Röthlisberger, and D. Loss, Phys. Rev. A **82**, 022305 (2010).
[10] F. L. Pedrocchi, S. Chesi, and D. Loss, Phys. Rev. B **84**, 165414 (2011).
[11] D. I. Tsomokos, T. J. Osborne, and C. Castelnovo, Phys. Rev. B **83**, 075124 (2011).
[12] J. R. Wootton and J. K. Pachos, Phys. Rev. Lett. **107**, 030503 (2011).
[13] C. Stark, L. Pollet, A. Imamoğlu, and R. Renner, Phys. Rev. Lett. **107**, 030504 (2011).
[14] S. Bravyi and R. Koenig, e-print arXiv:1108.3845.
[15] A. R. Calderbank and P. W. Shor, Phys. Rev. A **54**, 1098 (1996).
[16] A. M. Steane, Proc. R. Soc. London, Ser. A **452**, 2551 (1996).
[17] E. B. Davies, Commun. Math. Phys. **39**, 91 (1974).
[18] R. Alicki, M. Fannes, and M. Horodecki, J. Phys. A **42**, 065303 (2009).
[19] A. J. Leggett, S. Chakravarty, A. T. Dorsey, M. P. A. Fisher, A. Garg, and W. Zwerger, Rev. Mod. Phys. **59**, 1 (1987).
[20] D. P. DiVincenzo and D. Loss, Phys. Rev. B **71**, 035318 (2005).
[21] J. Edmonds, Can. J. Math. **17**, 449 (1965).
[22] V. Kolmogorov, Math. Prog. Comput. **1**, 43 (2009).
[23] J. R. Shewchuk, in *Applied Computational Geometry: Towards Geometric Engineering*, Lecture Notes in Computer Science Vol. 1148, edited by M. C. Lin and D. Manocha (Springer-Verlag, Berlin, 1996), pp. 203–222.
[24] Note that f_{cr}^{Z} could equivalently be obtained from dynamical simulations in the presence of a bath with constant error rates at the time where the error-corrected logical Z operators for different system sizes intersect.
[25] M. Ohzeki, Phys. Rev. E **79**, 021129 (2009).
[26] D. Gottesman and H.-K. Lo, IEEE Trans. Inf. Theory **49**, 457 (2003).
[27] Note that the error correction is unaware of the distribution of negative and positive on-site energies. If it were, this information could in principle be used to improve the lifetime of the memory.
[28] S. Bravyi, M. B. Hastings, and S. Michalakis, J. Math. Phys. **51**, 093512 (2010).
[29] S. Dusuel, M. Kamfor, R. Orus, K. P. Schmidt, and J. Vidal, Phys. Rev. Lett. **106**, 107203 (2011).
[30] A. Kay, Phys. Rev. Lett **102**, 070503 (2009).
[31] F. Pastawski, A. Kay, N. Schuch and I. Cirac, Quantum Inf. Comput. **10**, 580 (2010).
[32] P. W. Anderson, Phys. Rev. **109**, 1492 (1958).
[33] X. Feng, Y. Deng, and H. W. J. Blöte, Phys. Rev. E **78**, 031136 (2008).